

PAPER • OPEN ACCESS

Modelling viscoplastic behavior of solidifying shell under applied electromagnetic breaking during continuous casting

To cite this article: A Vakhrushev *et al* 2020 *IOP Conf. Ser.: Mater. Sci. Eng.* **861** 012015

View the [article online](#) for updates and enhancements.

Modelling viscoplastic behavior of solidifying shell under applied electromagnetic braking during continuous casting

A Vakhrushev¹, A Kharicha¹, M Wu², A Ludwig², G Nitzl³, Y Tang³, G Hackl³, J Watzinger⁴ and C M G Rodrigues²

¹ Christian-Doppler Lab for Metallurgical Applications of Magnetohydrodynamics, University of Leoben, Franz-Josef-Str. 18, A-8700 Leoben, Austria

² Chair of Simulation and Modeling of Metallurgical Processes, University of Leoben, Franz-Josef-Str. 18, A-8700 Leoben, Austria

³ RHI Magnesita, Austria

⁴ Primetals Technologies, Austria

E-mail: alexander.vakhrushev@unileoben.ac.at

Abstract. Since several decades the continuous casting (CC) process became one of the dominant technologies for the metal production. The quality optimization and the production rate growth are the primary targets. Nowadays the numerical modelling is a valuable tool to assist in these aims. Moreover, it efficiently competes with the physical experiment and the industrial trials. One of the key issues with the high casting speeds especially for the thin slab products are the strong turbulent flow of the fresh melt being feed from the submerged entry nozzle (SEN) and the non-uniformity of the solidifying shell thickness. Thereby the electromagnetic braking (EMBr) is typically applied to damp the hot jets and to evenly redistribute the superheat. In the previous work it was shown by the authors that the presence of the highly conductive solid shell plays crucial role for the melt flow under the applied magnetic field. Excluding this interaction does not allow predicting the EMBr effects on the melt flow correctly during the solidification. Recently a viscoplastic deformation model was implemented to model a withdrawal of the solidified shell in a funnel type CC mold for a full 3D engineering geometry. An extended model was used to predict the macro-segregation during twin-roll casting of an Al-alloy using 2D assumption due to the large width / thickness ratio of the casted sheet. In the current study an effort is done to combine the viscoplastic deformation model of the solidified shell and the magnetohydrodynamics effects of the EMBr. The flow field alternation as well as the thickness of the solidified shell during CC are presented and analyzed with and without the magnetic field been applied.

1. Introduction

The thin slab casting (TSC) of steel is an effective continuous casting (CC) technology, featuring high casting speeds, reduced macrosegregation, applicability in the direct rolling concept and significant energy savings. However, the development of a highly turbulent flow in a narrow funnel-shape mold causes instability of the meniscus, the local remelting and thinning of the shell and enhanced risk of the slag and non-metallic inclusions entrapment. The electromagnetic brake (EMBr) is one of the widely applied flow control techniques [1]. Along with that, the numerical simulation became a valuable tool to investigate and to optimize this technology for the foundry field, whereas the immediate observation of the EMBr effects is mostly impossible at the real casting mill.



The mechanical properties of the alloys drastically vary in the two phase region [2]. Recently a viscoplastic deformation model was implemented by the current work authors with an aim to reflect this phenomenon during a withdrawal of the solidified shell in a funnel type CC mold [3]. Next, an extended two-phase approach was used to predict the macro-segregation during twin-roll casting of an Al-alloy sheets [4].

In current work the solidification model considering viscoplastic Norton-Hoff stress in the solidified shell is for the first time combined with the magnetohydrodynamics (MHD) Lorentz force. It is applied to simulate a thin slab casting process including a submerged entry nozzle (SEN) region, the mold and the strand part. The coupling is done using mixture volume averaging combining previously developed models [3, 5] with the MHD model based on the electric potential method [6]. The alternation of the liquid melt flow and the solidified shell thickness under the applied EMBR is simulated and discussed in the presented study.

2. Numerical model

2.1. General equations

Current work uses a constant density assumption for the solidifying melt. Thereby the incompressible mixture volume averaging gives the following continuity and momentum equations:

$$\nabla \cdot \mathbf{u} = 0, \quad (1)$$

$$\rho \left[\frac{\partial \mathbf{u}}{\partial t} + \nabla \cdot (\mathbf{u} \otimes \mathbf{u}) \right] = \nabla \cdot [\text{dev}(\boldsymbol{\Sigma}_{\text{tot}}) - p\mathbf{I}] + \mathbf{F}_L. \quad (2)$$

The deviatoric part of the total stress $\boldsymbol{\Sigma}_{\text{tot}}$ combines the viscoplastic $\boldsymbol{\Sigma}^{\text{vp}}$ and the Newtonian stresses based on the solid f_s and liquid f_ℓ phase fractions:

$$\text{dev}(\boldsymbol{\Sigma}_{\text{tot}}) = f_s \cdot \boldsymbol{\Sigma}^{\text{vp}} + f_\ell \cdot 2\mu_\ell \cdot \text{dev}(\dot{\boldsymbol{\epsilon}}). \quad (3)$$

No turbulence modelling is used in the current study, thus the liquid viscosity μ_ℓ is assumed to be constant. The Lorentz force \mathbf{F}_L in equation (2) represents magnetohydrodynamics effects from the applied magnetic field.

2.2. Viscoplastic behavior of the solidified shell

The detailed implementation of the mixture-based deformation model was previously described by the authors in reference [3] based on the hot steel viscoplastic behavior assumption from the book of Rappaz and coauthors [7]. Excluding the compressibility of the mush [8, 9], the solidifying shell is considered as an incompressible ‘creeping solid’. The Norton-Hoff viscoplastic stress model combines the strain rate tensor and the equivalent strain rate as

$$\boldsymbol{\Sigma}^{\text{vp}} = 2K(\sqrt{3} \dot{\epsilon}_{\text{eq}})^{m-1} \text{dev}(\dot{\boldsymbol{\epsilon}}) \quad (4)$$

with the viscoplastic consistency K and strain rate sensitivity m being the model parameters [3, 7]. Full coupling between the deformation model (4) with the momentum equation (2) is done in the iterative manner by employing the improved both-side diffusion method to promote the stress-velocity coupling to overcome the stiffness of the stress tensor term [10].

2.3. Solidification model

To consider the solidification and the formation of the shell during the continuous casting the energy equation for the temperature T is taken as

$$\rho C_p \left[\frac{\partial T}{\partial t} + \nabla \cdot (\mathbf{u} T) \right] = \nabla \cdot \lambda \nabla T + S_e, \quad (5)$$

where the latent heat advection term is

$$S_e = \rho L \left[\frac{\partial f_s}{\partial t} + \nabla \cdot (f_s \cdot \mathbf{u}) \right]. \quad (6)$$

with the specific heat C_p and the latent heat of fusion L .

2.4. Modelling magnetohydrodynamics effects

The Lorentz force \mathbf{F}_L in momentum equation (2) is a cross product of the induced current density \mathbf{j} and the externally applied magnetic field \mathbf{B}_0 :

$$\mathbf{F}_L = \mathbf{j} \times \mathbf{B}_0. \quad (7)$$

The electric potential method is applied for the Maxwell's equations closure [11]. By introducing the electric potential φ , the e-current \mathbf{j} can be calculated from the Ohm's law:

$$\mathbf{j} = \sigma(-\nabla\varphi + \mathbf{u} \times \mathbf{B}_0), \quad (8)$$

where σ is the electrical conductivity. The e-potential φ is calculated from the corresponding Poisson equation:

$$\nabla \cdot (\sigma \nabla\varphi) = \nabla \cdot (\sigma (\mathbf{u} \times \mathbf{B}_0)), \quad (9)$$

Electric conductivity σ is considered to vary ~ 1.4 times between liquid melt and solidified shell. The combined MHD / solidification solver is developed in the open-source CFD package OpenFOAM® [12]. According to the numerical model described in equations (1)–(9) a corresponding solver including fluid flow, viscoplastic stresses in the shell and action of the Lorentz force was developed. The MHD model is previously verified with the experimental measurements [13]. Initial studies for the influence of the highly conductive solid were presented in Liu *et al.* [14].

3. Simulation results

The combined model considering solidification, viscoplastic behavior of the shell and the effect of the EMBr was applied for the simulation of the thin slab casting process. The schematics of the simulated domain including SEN, primary (mold) and secondary (slab) cooling zones is shown in figure 1(a). The heat flux distribution along the casting direction is plotted in figure 1(b). The growth of the solidified shell is represented by solid fraction / temperature curve in figure 1(c). The magnetic field distribution of the 3-pole EMBr applied across the mold at 560 mm below meniscus with the peak value of 188 mT is in figure 1(d). The EMBr is aligned to act in the area of the side and central jets coming out of the 4 port SEN. All boundaries excluding domain's outlet and inlet are electrically insulated.

The 0.06C 0.1Ni 0.13Mn 0.1Si 0.08Cu 0.035Al 0.015P 0.012S alloy properties, the applied electromagnetic brake settings and casting conditions are listed in table 1. Viscoplastic model parameters correspond to the Model IA in Kozłowski *et al.* [15] and are previously analyzed and presented by the authors in [3].

The numerical mesh is originally refined near the mold walls and the slab water cooled surface to correctly resolve the temperature gradient. After the solidified shell develops an additional refinement is done at the region of the mushy zone based on the time averaged results. All in all, the mesh size reaches 10 million cells. The time integration step is adjusted dynamically to keep Courant number below 1.

The results of the thin slab CC simulation are shown in figures 2-4. The comparison between the no EMBr case and with the applied magnetic field is done. Firstly, the flow field alternation is presented in figure 2. For the no EMBr case a developed double-roll pattern is observed with the strong side and central jets (see figure 2(b)). When the EMBr is applied, the strong braking of the flow occurs. The jets become more stable, no impinging on the narrow walls is observed as can be seen in figure 2(c). At the lower part of the mold and in the slab region the melt flow becomes more uniform. The sub-meniscus velocities are reduced as well.

Table 1. Alloy properties, EMBr settings and casting conditions.

Properties	Symbols	Units	Quantities
Alloy density	ρ	kg m^{-3}	6998.49
Specific heat	C_p	$\text{J kg}^{-1} \text{K}^{-1}$	838.2
Thermal conductivity	λ	$\text{W m}^{-1} \text{K}^{-1}$	35
Liquid dynamic viscosity	μ_l	Pa s	0.0054
Latent heat of fusion	L	J kg^{-1}	243000
Viscoplastic consistency	K	Pa s^m	65.16
Strain rate sensitivity	m	–	0.138
Electrical conductivity:	σ	S m^{-1}	
liquid melt			770000
solidified shell			1075000
Casting velocity	\mathbf{u}_{pull}	m min^{-1}	4.3
Casting (inlet) temperature	T_{cast}	$\text{K } (^{\circ}\text{C})$	1825 (1552)
Liquidus temperature	T_{liquidus}	$\text{K } (^{\circ}\text{C})$	1798 (1525)
Solidus temperature	T_{solidus}	$\text{K } (^{\circ}\text{C})$	1755 (1482)
EMBr magnetic field	\mathbf{B}_0	mT	188

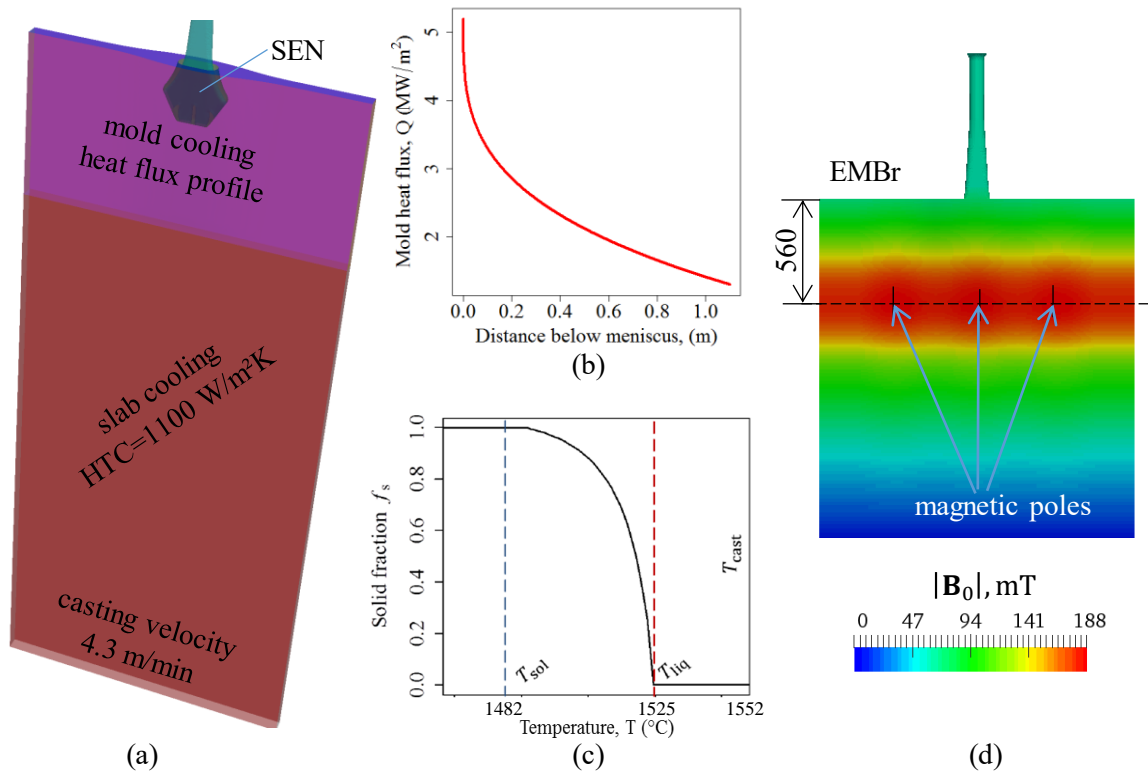


Figure 1. Simulation setup: (a) numerical domain layout with the cooling and casting conditions; (b) mold heat flux profile; (c) solid fraction vs. temperature curve; (d) applied EMBr magnetic field.

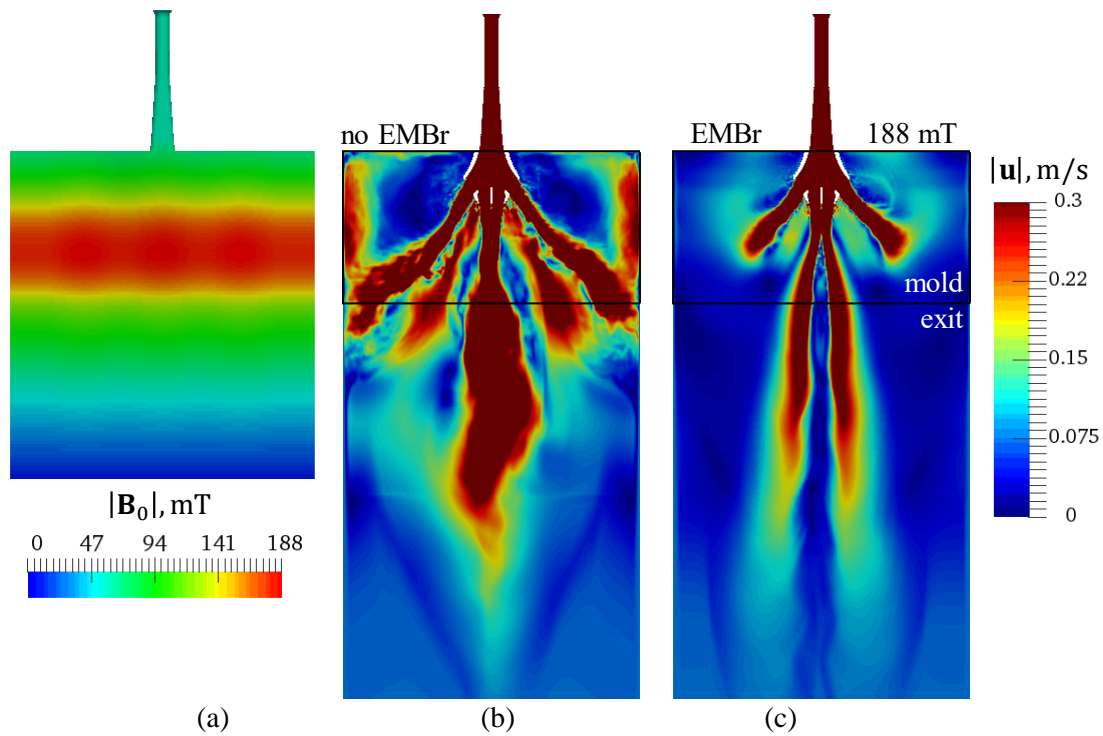


Figure 2. The simulated (instantaneous) flow field for the thin slab casting: (a) applied magnetic field distribution; (b) velocity magnitude distribution in the mid-plane without and (c) with applied EMBR.

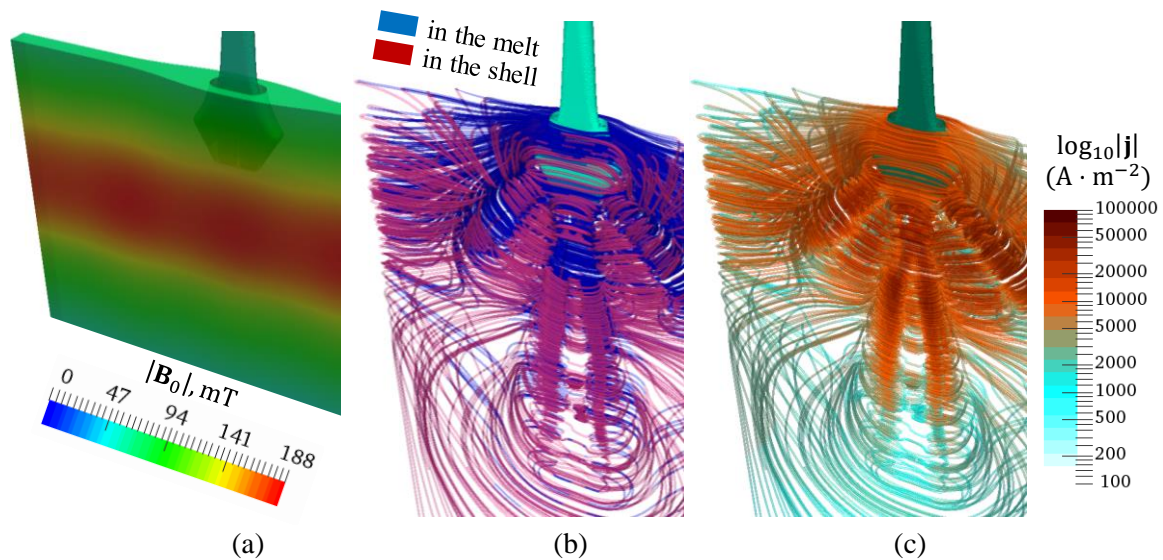


Figure 3. The induced current density lines: (a) applied magnetic field distribution; (b) e-current lines located in the liquid bulk (blue) and conducted through the solid shell (red); (c) e-current lines with the corresponding induced current density magnitude.

The strong braking action of the Lorentz force occur due to the fact, that the induced current density lines tend to close in the form of loops through the more conductive solid shell, which is indicated in figure 3(b) by corresponding colors. Thereby the e-current lines are “attached” to the shell and do not allow to develop the flow instabilities. At the same time, it is observed, that the most e-current is generated in the jets regions and is concentrated in the upper part of the domain.

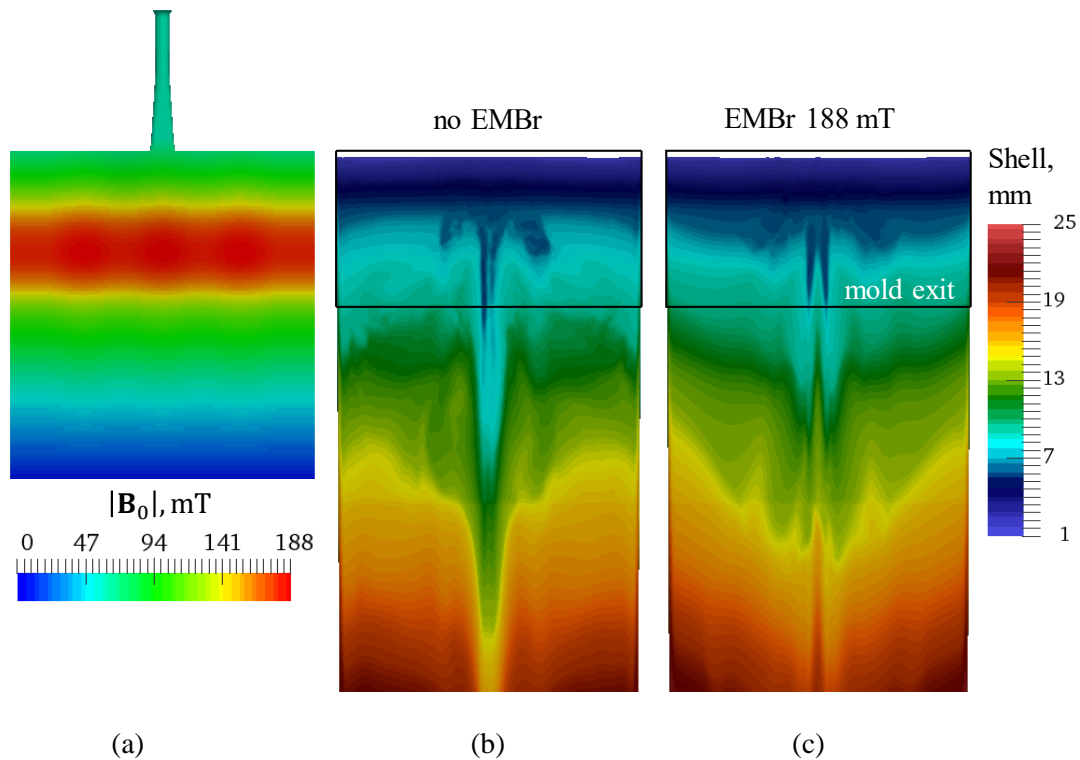


Figure 4. The simulated (instantaneous) solid shell for the thin slab casting: (a) applied magnetic field distribution; (b) shell thickness along a wide face without and (c) with applied EMBR. Results are shown for the 100% solid fraction iso-surface.

The corresponding changes of the hot melt flow consequently lead to the improved solid shell growth. The shell thickness is displayed in figure 4 representing the iso-surface of 100% solid fraction. For the initial configuration with no EMBR (figure 4(b)) the strong remelting of the shell is observed in the region of the side jets and at the center of the mold's wide side. The shell thickness is strongly non-uniform in the longitudinal and especially in the transversal direction. By applying the EMBR due to the flow pattern improvement and because of the braking effect, the shell thickness becomes significantly even. However further increase of the magnetic field value will lead to the formation of the opposite meniscus roll, thereby the EMBR should be combined with the advanced SEN designs. This topic as well as the interaction of the applied magnetic field with the viscoplastic stresses in the shell are the subjects for the future studies.

4. Conclusions

In the presented study the solidification model including a viscoplastic stress in the two-phase region was newly combined with the magnetohydrodynamics Lorentz force. Full coupling is done in the iterative manner including: modelling of the liquid melt flow; motion of the solidifying shell under a withdrawal according to the Norton-Hoff relation for the deviatoric stress tensor; the electromagnetic braking due to the induced electric current density under the applied magnetic field.

The effect of the applied EMBR on the flow pattern and the solidifying shell thickness for the real 3D geometry of the thin slab caster was investigated. The reduction of the hot melt impingement on the solidification front was observed, leading to more uniform solid shell profile. The developed methodology can be applied for the wide range of the EMBR settings and different mold / SEN designs to investigate the meniscus profile and fluctuations along with the submeniscus velocities, which are important reasons for applying EMBR technique.

Acknowledgments

The authors acknowledge the financial support by the Austrian Federal Ministry of Economy, Family and Youth and the National Foundation for Research, Technology and Development within the framework of the Christian Doppler Laboratory for Metallurgical Applications of Magnetohydrodynamics.

References

- [1] Thomas B G and Cho S M 2018 *IOP Conf. Ser.: Mater. Sci. Eng.* **424** 012027
- [2] Flemings M C 1991 *Metall. Trans. A* **22A** 957–81
- [3] Vakhrushev A, Kharicha A, Wu M, Ludwig A, Nitzl G, Tang Y, Hackl G, Watzinger J and Rodrigues C M G 2019 *IOP Conf. Ser.: Mater. Sci. Eng.* **529** 012081
- [4] Rodrigues C M G, Ludwig A, Kharicha A, Wu M and Vakhrushev A 2019 *Metall. Mater. Trans. B* **50** 1334–50
- [5] Vakhrushev A, Wu M, Ludwig A, Tang Y, Hackl G and Nitzl G 2014 *Metall. Mater. Trans. B* **45B** 1024–37
- [6] Vakhrushev A, Kharicha A, Liu Z, Wu M, Ludwig A, Nitzl G, Tang Y, Hackl G and Watzinger J 2019 *STEELSIM Conf. Proceed.* **PR-503-064** 615
- [7] Rappaz M, Bellet M and Deville M 2003 *Numerical Modeling in Materials Science and Engineering* (New York: Springer) chapter 6 p 309
- [8] Fachinotti V D, Le Corre S, Triolet N, Bobadilla M and Bellet M 2006 *Int. J. Numer. Meth. Engng.* **67** 1341–84
- [9] Bellet M 2007 *AIP Conf. Proc.* **908:1** 1369–74
- [10] Fernandes C, Araujo M S B, Ferrás L L and Nóbrega J M 2017 *J. Non-Newtonian Fluid Mech.* **249** 63–78
- [11] Davidson P 2001 *An Introduction to Magnetohydrodynamics* (Cambridge: Cambridge University Press) chapter 9 p 304
- [12] Weller H G, Tabor G, Jasak H and Fureby C 1998 *Comput. Phys.* **12(6)** 620–31
- [13] Thomas B G, Singh R, Vanka S P, Timmel K, Eckert S and Gerbeth G 2015 *J. Manuf. Sci. Prod.* **15(1)** 93–104
- [14] Liu Z, Vakhrushev A, Wu M, Karimi-Sibaki E, Kharicha A, Ludwig A and Li B 2018 *Metals* **8** 609
- [15] Kozłowski P F, Thomas B G, Azzi J A and Wnag H 1992 *Metall. Mater. Trans B* **23A** 903–18